

Friction Coefficient of an Intact Free Liquid Jet Moving in Air

P.M. Comiskey, and A.L. Yarin*

Department of Mechanical and Industrial Engineering, University of Illinois at Chicago, 842 W.

Taylor St., Chicago IL 60607-7022, U.S.A.

*Corresponding author: ayarin@uic.edu

Acknowledgement

This work was financially supported by the US National Institute of Justice (NIJ 2017-DN-BX-0171).

Abstract

Here we propose a novel method of determining the friction coefficient of intact free liquid jets moving in quiescent air. The middle-size jets of this kind are relevant for such applications as decorative fountains, fiber forming, fire suppression, agriculture and forensics. The present method is based on measurements of trajectories created using a straightforward experimental apparatus emulating such jets at a variety of initial inclination angles. Then, the trajectories are described theoretically, accounting for the longitudinal traction imposed on such jets by the surrounding air. The comparison of the experimental data with the theoretical predictions show that the results can be perfectly superimposed with the friction coefficient $C_{fd} = 5Re_d^{-1/2 \pm 0.05}$, in the $621 \leq Re_d \leq 1289$ range, with Re_d being the Reynolds number based on the local cross-sectional diameter of the jet. The results also show that the farthest distance such jets can reach corresponds to the initial inclination angle $\alpha = 35^\circ$ which is in agreement with already published data.

1. Introduction

Free liquid jets moving in air are a common phenomenon since decorative fountains, fire extinguishers and different sprinklers are frequently seen in our everyday life. One of the first studies attempting to better understand free liquid jets was sensibly related to large water jets used to suppress fires (Freeman 1889). This extensive work quantified friction loss in hoses, roughness of various nozzles, effects due to backpressure, and even attempted to formulate a simple theory to match the trajectories of large firefighting jets. Practical nozzle designs were

further discussed by Rouse et al. (1951), Arato et al. (1970), and Theobald (1981), which, in particular, made additional theoretical predictions of jet trajectories using a model based on projectile motion neglecting air resistance. Early work in the field was dominated by experimental tests intended to design the best fire suppression or agricultural systems (Bilanski and Kidder 1958). It resulted in many practically important observations such as the optimal (determined by the maximum range reached by liquid) initial inclination angle of the jet in the 30-40° range reported by Hatton and Osborne (1979) or 35° reported by Theobald (1981).

Theoretically, the trajectories of liquid jets have often been predicted using the equations of projectile motion where air resistance is either neglected (Rouse et al. 1951, Wahl et al. 2008) or empirically accounted for (Hatton and Osborne 1979, Hatton et al. 1985). This results in trajectories which form parabolic arcs (Tuck 1976, Hatton and Osborne 1979, Hatton et al. 1985, Clanet 1998), even though the effect of the aerodynamic drag has been used to explain the difference between theory and experiments (Clanet 1998). For large sprinkler jets it was found that air drag should be accounted for as Murzabaev and Yarin (1985) showed in their numerical model of multiphase turbulent atomizing jets. Recently, Trettel and Ezeokye (2015) developed a theoretical model which assumes the jet to be intact and unaffected by air drag until a breakup point, at which the jet instantaneously becomes a droplet train system whose motion is affected by air drag. Moreover, for the multiphase atomizing jets relevant in agricultural and forensic applications it was shown that the aerodynamic drag experienced by individual drops is determined by their corrective interaction similarly to the aerodynamic interaction of birds flying in V formation (Lissaman and Shollenberger 1970, Murzabaev and Yarin 1985, Comiskey et al. 2017b).

Liquid in free liquid jets can either be Newtonian, such as water in decorative fountains and sprinklers, or non-Newtonian as in fiber forming processes (Ziabicki 1976, Ziabicki and Kawai 1985) and in intact jets of blood which can form when a sharp object lacerates a main blood vessel (Wonder 2001, Hanson 2004, James et al. 2005). The latter situation is of particular interest to the present group, which dealt before with multiphase blood spatter jets resulting from a gunshot (Comiskey et al. 2016, 2017a, 2017b, 2018). The ejection of intact blood jets is called arterial gushing and originates from a high pressure location within the body such as the neck (Wonder 2001, James et al. 2005). Such phenomena can occur when knives or other cutting instruments are used as a murder weapon, which, is on the rise. In the United States, knives or other cutting instruments accounted for 12.9% of murders in 2005 and 13.1% in 2014, even though violent crime was down 16.2% during that period (Federal Bureau of Investigation 2005, 2014).

The transition from dripping to an intact liquid jet can happen at a large enough outflow velocity (Yarin 1993, Clanet and Lasheras 1999). As the outflow velocity increases, such jets break up due to the surface-tension-driven capillary instability, then, at a higher velocity, by the bending instability and the atomization process, with the latter two mechanisms being driven by the dynamic interaction with the surrounding air (Rayleigh 1878, Rutland and Jameson 1971, Basaran 1992, Yarin 1993, Lin and Reitz 1998, Clanet and Lasheras 1999, Ashgriz and Yarin 2011, Yarin 2011, Yarin et al. 2014, 2017). Free jets of non-Newtonian polymeric liquids in many practically important applications are unaffected by these instabilities and stay intact even though their velocities of motion relative to air are very high, for example in fiber forming processes such as melt spinning, solution and melt blowing, etc. (Ziabicki 1976, Ziabicki and Kawai 1985, Yarin 1993, Yarin et al. 2014 and references therein). Accordingly, in this latter

group of works, the significant effect of the coefficient of friction drag acting on elongated cylindrical bodies was in focus. It was established that it cannot be described by the standard Blasius or Schultz-Grunow and other theoretical and empirical correlations based on the boundary layer theory and dependent on the Reynolds number based on the longitudinal length scale (Schlichting 1979). In the case of elongated cylindrical bodies, the boundary layer thickness becomes larger than the cross-sectional diameter, and as a result, the average friction coefficient is determined by the Reynolds number based on the diameter, Re_d , rather than on the longitudinal scale. Accordingly, several semi-empirical and empirical correlations for the friction coefficient of intact straight solid cylinders (wires) or liquid jets moving in air were established in the $0.04 \leq Re_d \leq 400$ range. For example, Glicksman (1968) proposed the expression for the friction coefficient in the form of $C_{fd} = 0.4Re_d^{-0.7}$, while Yarin (1992, 1993) employed $C_{fd} = 0.65Re_d^{-0.81}$, where the dimensionless friction coefficient is defined as the friction force (traction) T , rendered dimensionless by the product of the jet surface area S and the dynamic pressure of the surrounding air $\rho_a V_\tau^2 / 2$. Here ρ_a is the air density and V_τ is the tangential velocity of a liquid jet; also, the Reynolds number is defined as $Re_d = 2aV_\tau / \nu_a$, with $d=2a$ being the cross-sectional jet diameter (with the radius denoted as a), and ν_a being the kinematic viscosity of air. Several other works in which a wire was either supported in a wind tunnel, or was moving through air at rest resulted in the expressions of the type $C_{fd} = \gamma Re_d^{-\beta}$, with γ in the 0.23-1.78 range and β in the 0.62-0.81 range valid in different intervals of Re_d in the 5-400 range (Ziabicki 1976, Ziabicki and Kawai 1985, and references therein). The applicability of these expressions for the average friction coefficient to curved intact free liquid jets arising in

decorative fountains, sprinklers and forensic applications has never been examined. An *ad hoc* hypothesis of their applicability is questionable.

The internal geometry of the nozzle is one of the most fundamental components in the formation of an intact free liquid jet. In such applications as decorative fountains and small sprinklers, the nozzles are typically designed to provide a gradual transition toward the exit and are operated with a backpressure which keeps the working fluid attached to the nozzle walls. If the working fluid becomes detached from the nozzle walls, however, a constricted jet can be created. Such a jet can travel distances further than normally obtained because the destabilizing effects from the nozzle walls are eliminated (Tafreshi and Pourdeyhimi 2003). Such jet detachments appear on sharp orifices and stiff nozzle generatrices, e.g. of the so-called Borda mouthpiece (de Borda 1766), and result from an essentially inviscid flow kinematics (leading to vena contracta) supplemented by the momentum balance in the form of the Bernoulli equation (Lamb 1959, Kochin et al. 1964). The nozzles used in the present experiments did not create constricted jets, because their internal geometry closely followed that of a pressure washer except designed to work at a low backpressure.

The present work aims at establishing the average friction coefficient of intact liquid jets moving in air under the conditions characteristic of decorative fountains, smaller sprinklers and forensic applications, which are drastically different from those in melt spinning and in the above-mentioned experiments with wires.

2. Experiment

Intact jets were experimentally issued using a three-tier nozzle system (Fig. 1). The working fluid was kept in a storage vessel and supplied to the nozzle system using a submerged circulation pump (Marineland Maxi-Jet 600). The first tier of the nozzle system which the working fluid encountered consisted of a porous medium which acted to smooth the pulsing, slightly-transient flow from the circulation pump. Then, the second stage was an elongated honeycomb mesh intended to prevent any possible swirling or secondary flows. The final stage consisted of an enclosed cavity which filled uniformly and smoothly as it supplied the working fluid into the nozzle. Two different solid-stream spray nozzles with cross-sectional areas of 0.04 cm^2 and 0.13 cm^2 (McMaster-Carr 7611T43 and 7611T46), were used. The free liquid jets were collected in a second storage vessel which had another submerged circulation pump (Marineland Maxi-Jet 600) to pump the working fluid back to the first storage tank, thus creating a closed-loop system schematically shown in Fig. 1.

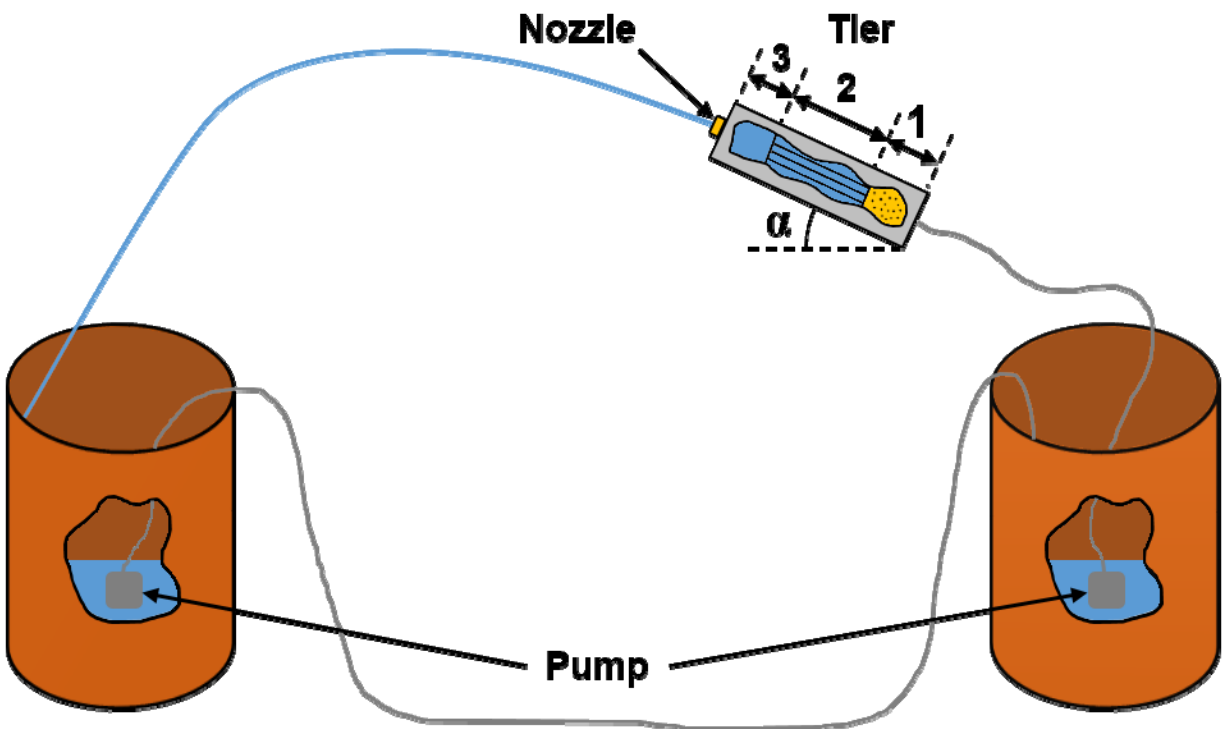


Fig. 1. Schematic of the experimental setup. The free liquid jet issued from the nozzle is shown in blue, whereas the gray lines indicate tubing. Tier 1 corresponds to the porous medium, tier 2 is the elongated honeycomb mesh, and tier 3 is the enclosed cavity.

There were 2 replicated experiments, one for each nozzle type with 4 different initial inclination angles, with a total of 9 experiments listed in Table 1. The two nozzle types were tested at the initial inclination angles of $\alpha \approx 0^\circ$, 20° , 40° , and 60° . The inclination angle values were measured with a digital level on site and later corrected to more precise values based upon the images taken during each experiment, which resulted in the corrected values listed in Table 1. The pressure head between the first submerged circulation pump and the nozzle system had to be overcome by the pump, which sustained a nearly constant flow rate. Accordingly, simply raising the three-tiered nozzle system reduced the flow rate of the working fluid through the nozzle. As a result, low-velocity jet experiments could easily be performed by inducing in this way a large opposite pressure head as is the case of experiment 9 in Table 1. Note that for all other experiments, the pressure head was effectively kept constant, however, slight deviations led to a difference in jet velocity even for the same nozzle type. The velocity was determined through measuring the volumetric flow rate approximately 30 times for each experiment and using the known nozzle outlet area. The values were then averaged, with the results and the corresponding standard deviations being listed in Table 1. No discharge coefficients were needed in this calculation because the internal geometry of the nozzles was smooth and gradual resulting in a discharge coefficient very close to unity, which was corroborated by the jet images of the type shown in Fig. 2. The working fluid used in all experiments was water.

Table 1. Experimental parameters. Note that the values of α listed here were measured from experimental images and Re_d is the jet Reynolds number based on the jet velocity, diameter at the nozzle exit, and the kinematic viscosity of air.

Experiment Number	Cross-sectional Nozzle Area [cm ²]	α [deg]	Jet Velocity [cm/s]	Re_d
1	0.04	2.00	438.69 ± 12.78	743
2	0.04	19.00	412.85 ± 5.96	652
3	0.04	38.73	404.22 ± 6.08	650
4	0.04	58.28	390.38 ± 7.63	621
5	0.13	-4.14	398.29 ± 12.8	1180
6	0.13	22.87	422.82 ± 19.37	1289
7	0.13	41.86	386.85 ± 15.05	1097
8	0.13	58.00	373.37 ± 9.96	1075
9	0.13	0.00	238.75 ± 8.46	713

3. Theoretical

The momentless quasi-one-dimensional theory of planar bending liquid jets yields the following continuity equation (1), and two projections (tangential and normal to the jet trajectory) of the momentum balance equation (Yarin 1993),

$$\frac{\partial \lambda f}{\partial t} + \frac{\partial f W}{\partial x} = 0, \quad (1)$$

$$\frac{\partial \lambda f V_\tau}{\partial t} - \frac{f V_n}{\lambda} \frac{\partial \lambda V_n}{\partial x} + \frac{\partial f V_\tau W}{\partial x} - \lambda f W k V_n = \frac{1}{\rho} \frac{\partial P}{\partial x} + \lambda f F_\tau + \frac{1}{\rho} \lambda q_\tau, \quad (2)$$

$$\frac{\partial \lambda f V_n}{\partial t} - \frac{f V_\tau}{\lambda} \frac{\partial \lambda V_n}{\partial x} + \frac{\partial f V_n W}{\partial x} + \lambda f W k V_\tau = \frac{1}{\rho} \lambda k P + \lambda f F_n + \frac{1}{\rho} \lambda q_n. \quad (3)$$

Here λ is the arc length of the jet axis, $\lambda = \sqrt{1 + (\partial H / \partial x)^2}$, H and x are the vertical and horizontal coordinates of the jet axis, f is the cross-sectional area of the jet, with the cross-section being approximately circular, and thus, $f = \pi a^2$, with a being the cross-sectional radius. Also, $W = V_\tau - V_n (\partial H / \partial x)$, with subscripts τ and n corresponding to the tangential and normal velocity components, respectively, k is the curvature of the jet axis, i.e. $k = (\partial^2 H / \partial x^2) \left[1 + (\partial H / \partial x)^2 \right]^{-3/2}$, ρ is the liquid density, F_τ and F_n denote the tangential and normal components of the acceleration associated with the body force (gravity, in the present case). Similarly, q_τ and q_n denote the tangential and normal components of the force imposed by the surrounding air on a unit length of the jet.

In the momentum balance, Eqs. (2) and (3), P is the longitudinal force acting in the jet cross-section given as

$$P = \left[3\mu \lambda^{-1} \partial V_\tau / \partial x - k V_n \text{sign}(\lambda^{-1} \partial V_\tau / \partial x - k V_n) - \sigma G \right] f + P_\sigma, \quad (4)$$

where μ is the liquid viscosity, σ is the surface tension, G is the double mean curvature of the surface of the jet, and $P_\sigma = 2\pi a \sigma \left[1 + \lambda^{-2} (\partial a / \partial x)^2 \right]^{-1/2}$. It should be emphasized that here the liquid is assumed to be Newtonian, as in the present experiments with water. For any other non-

Newtonian fluid [e.g. blood, which is pseudoplastic and viscoelastic, (Kolbasov et al. 2016)], Eq. (4) should be modified, as described in Yarin (1993).

For a steady state jet $\partial H/\partial t = \lambda V_n = 0$. Also, if the jet is thick enough, as in the present experiments, the effect of surface tension can be neglected. Then, Eqs. (1)-(4) take the following form

$$Q = fV_\tau, \quad (5)$$

$$\rho Q \frac{dV_\tau}{dx} = \frac{dP}{dx} + \rho \lambda f g_\tau + \lambda q_\tau, \quad (6)$$

$$\rho k f V_\tau^2 = kP + f \rho g_n, \quad (7)$$

$$P = 3\mu \frac{1}{\lambda} \frac{dV_\tau}{dx} f, \quad (8)$$

where Q is the volumetric flow rate in the jet.

Projecting the acceleration of the body force onto the normal and tangent to the jet axis (the trajectory arc), one obtains $g_n = -g/\lambda$, and $g_\tau = -g(1/\lambda)(dH/dx)$, respectively, with g being gravity acceleration. This transforms Eqs. (6) and (7) to the following form

$$\rho Q \frac{dV_\tau}{dx} = \frac{dP}{dx} - \rho f g \frac{dH}{dx} + \lambda q_\tau, \quad (9)$$

$$(\rho f V_\tau^2 - P)k = -\frac{f g \rho}{\lambda}. \quad (10)$$

In the steady-state case, the only non-zero tangential aerodynamic force, q_τ , acting on a unit jet length can be expressed as $q_\tau = -\tau_{\text{shear}} 2\pi a$, where τ_{shear} is the shear stress acting at the jet

surface. It is related to the friction coefficient C_{fd} as $\tau_{\text{shear}} = (1/2)\rho_a V_\tau^2 C_{fd}$. Also, noting that $a = \sqrt{Q/(V_\tau \pi)}$, Eqs. (9) and (10) are transformed to

$$\frac{d}{dx}(\rho Q V_\tau - P) = -\frac{\rho g Q}{V_\tau} \frac{dH}{dx} - \pi^{1/2} \lambda \rho_a V_\tau^{3/2} Q^{1/2} C_{fd}, \quad (11)$$

$$\frac{d^2 H}{dx^2} = -\frac{Q}{V_\tau} \frac{\rho g [1 + (dH/dx)^2]}{(\rho Q V_\tau - P)}. \quad (12)$$

Moreover, for water used in the present experiments, viscous effects can be essentially neglected, i.e. according to Eq. (8), $P=0$, which reduces the order of the differential equation relative to V_τ to the first one. Then, the boundary conditions for the system of Eqs. (11) and (12) are imposed only at the nozzle exit and read

$$x = 0: \quad V_\tau = V_{\tau 0}, \quad H = H_0, \quad \frac{dH}{dx} = \tan \alpha. \quad (13)$$

The governing equations, Eqs. (11) and (12) subjected to the boundary conditions (13) are solved numerically using Kutta-Merson with an automatically adjustable stepping in x .

4. Results and Discussion

The experimental apparatus described in Sect. 2 performs best with water as a working fluid. An image at the onset of the water jet used to determine the initial inclination angle and jet diameter is shown in Fig. 2(a), and an image of the trajectory arc of the water jet used to determine the experimental jet location is shown in Fig. 2(b).



Fig. 2. Images of the water jets used in experiment 5 (a) and experiment 8 (b).

The experimental results for the trajectories of water jets issued from the nozzle with the cross-sectional exit area of $f_0 = 0.04 \text{ cm}^2$ at the inclination angles of $\alpha = 19.00^\circ$, 38.73° , and 58.28° are shown in Fig. 3. The experimental results for the nozzle with the larger cross-sectional area, $f_0 = 0.13 \text{ cm}^2$, at the initial inclination angles of $\alpha = 22.87^\circ$, 41.86° , and 58.00° , are shown in Fig. 4. In the numerical simulations of the problem, Eqs. (11)-(13), the input velocities used were within the standard deviation of the experimentally measured values. The dependence for the friction coefficient was chosen as $C_{fd} = \gamma Re_d^{-\beta}$. The best fit of the predicted trajectories with the experimental data for all the experiments shown in Figs. 3, 4, and 5 was achieved with $\gamma = 5.0$ and $\beta = 1/2 \pm 0.05$, which means that the dependence $C_{fd} = 5Re_d^{-1/2 \pm 0.05}$ was established and it was uniformly valid for all experiments. Note that in Figs. 3 and 4 the experimental data are given for only the intact parts of the jets.

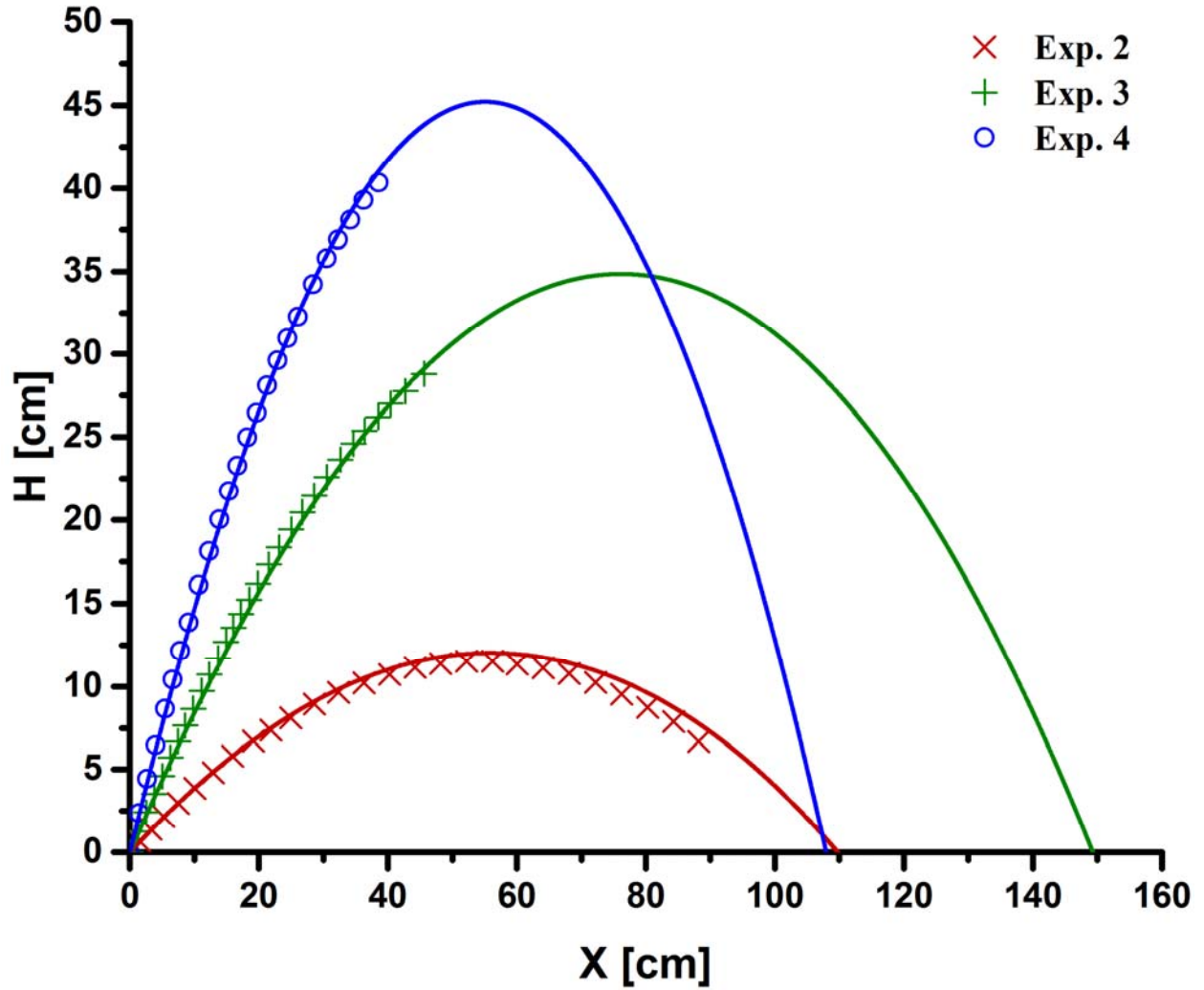


Fig. 3. Three superimposed trajectories for the intact free water jets. The legend refers to experiments 2 through 4 from Table 1. The experimental data are shown by symbols and solid lines correspond to the numerical predictions with $C_{fd} = 5Re_d^{-1/2 \pm 0.05}$.

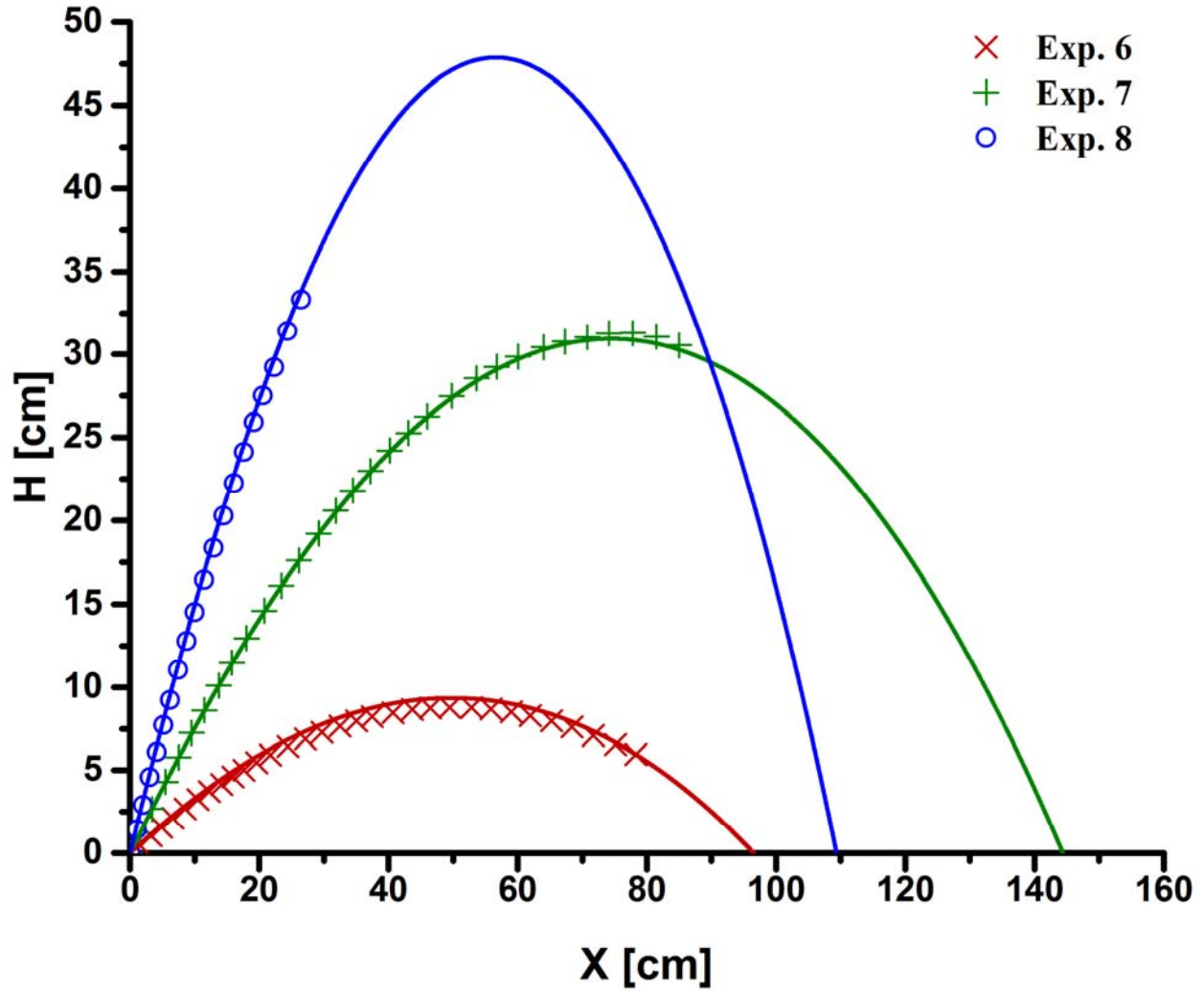


Fig. 4. Three superimposed trajectories for the intact free water jets. The legend refers to experiments 6 through 8 from Table 1. The experimental data are shown by symbols and solid lines correspond to the numerical predictions with $C_{fd} = 5Re_d^{-1/2 \pm 0.05}$.

The results for $f_0 = 0.04 \text{ cm}^2$ and 0.13 cm^2 with the corresponding initial angles of inclination of $\alpha = 2.00^\circ$ and -4.14° , respectively as well as for the low-velocity jet with

$f_0 = 0.13 \text{ cm}^2$ and $\alpha = 0.00^\circ$ are shown in Fig. 5. Here again, one finds the agreement of the predictions with the experimental data to be excellent when $C_{fd} = 5\text{Re}_d^{-1/2 \pm 0.05}$ is used.

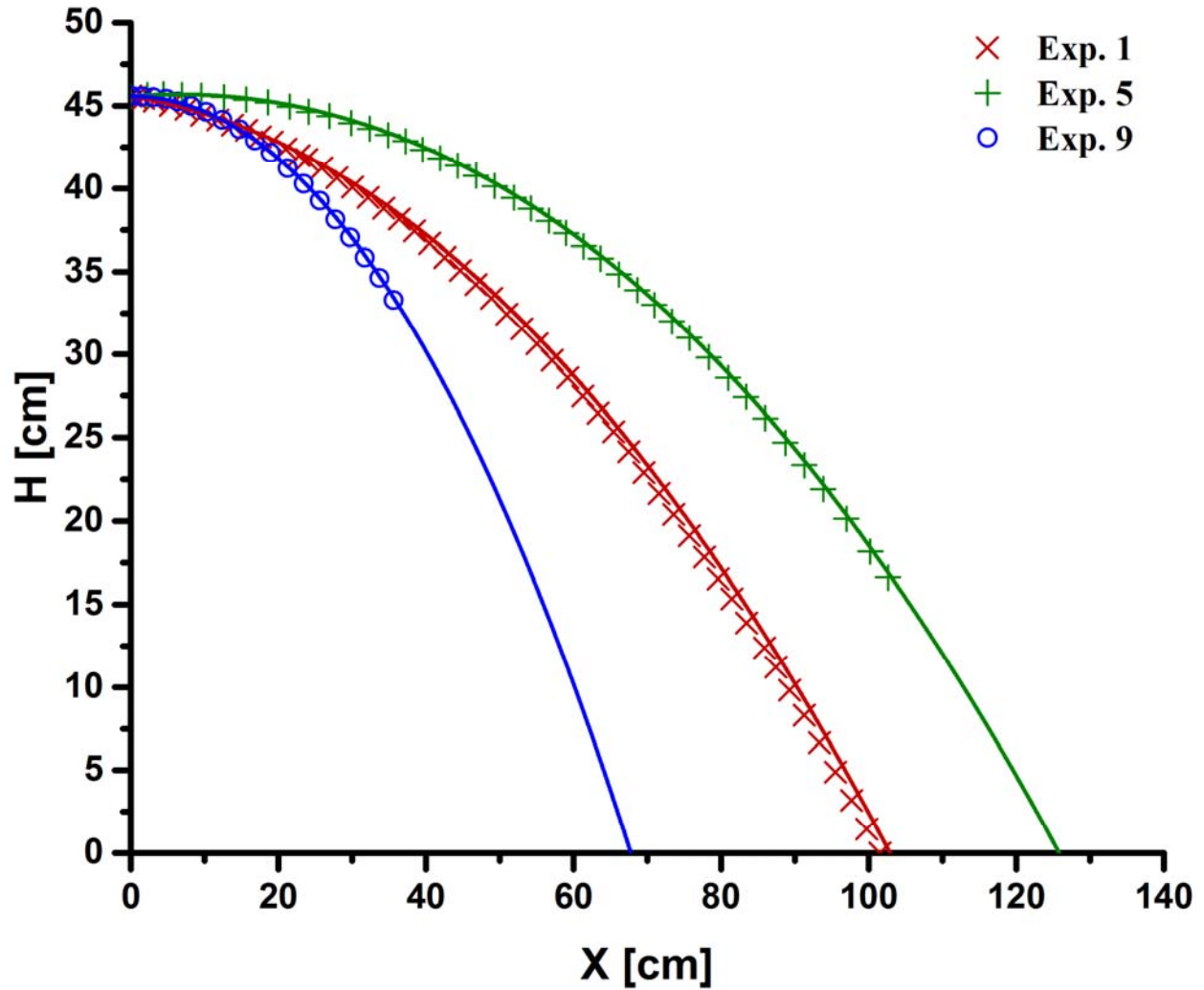


Fig. 5. Three superimposed trajectories for the intact free water jets. The legend refers to experiments 1, 5, and 9 from Table 1. The experimental data are shown by symbols and solid lines correspond to the numerical predictions with $C_{fd} = 5\text{Re}_d^{-1/2 \pm 0.05}$.

The accurate prediction of all jet trajectories with the uniformly valid friction coefficient $C_{fd} = 5Re_d^{-1/2 \pm 0.05}$ allows one to use the numerical simulations to find the optimal inclination angle for reaching the farthest distance. Figure 6 shows the corresponding results, which were obtained by varying only the initial inclination angle with the other parameters being fixed for two different jet Reynolds numbers corresponding to the experimentally studied range. Figure 6 reveals the optimal value of the inclination angle of $\alpha = 35^\circ$. This prediction is within the $\alpha = 30 - 40^\circ$ range of Hatton and Osborne (1979) and is in agreement with the experimental data of Theobald (1981) ($\alpha = 35^\circ$). Note also that the optimum angle is essentially the same as for the large scale two-phase sprinkler jets as shown by Murzbaev and Yarin (1985) where they found $\alpha = 36^\circ$.

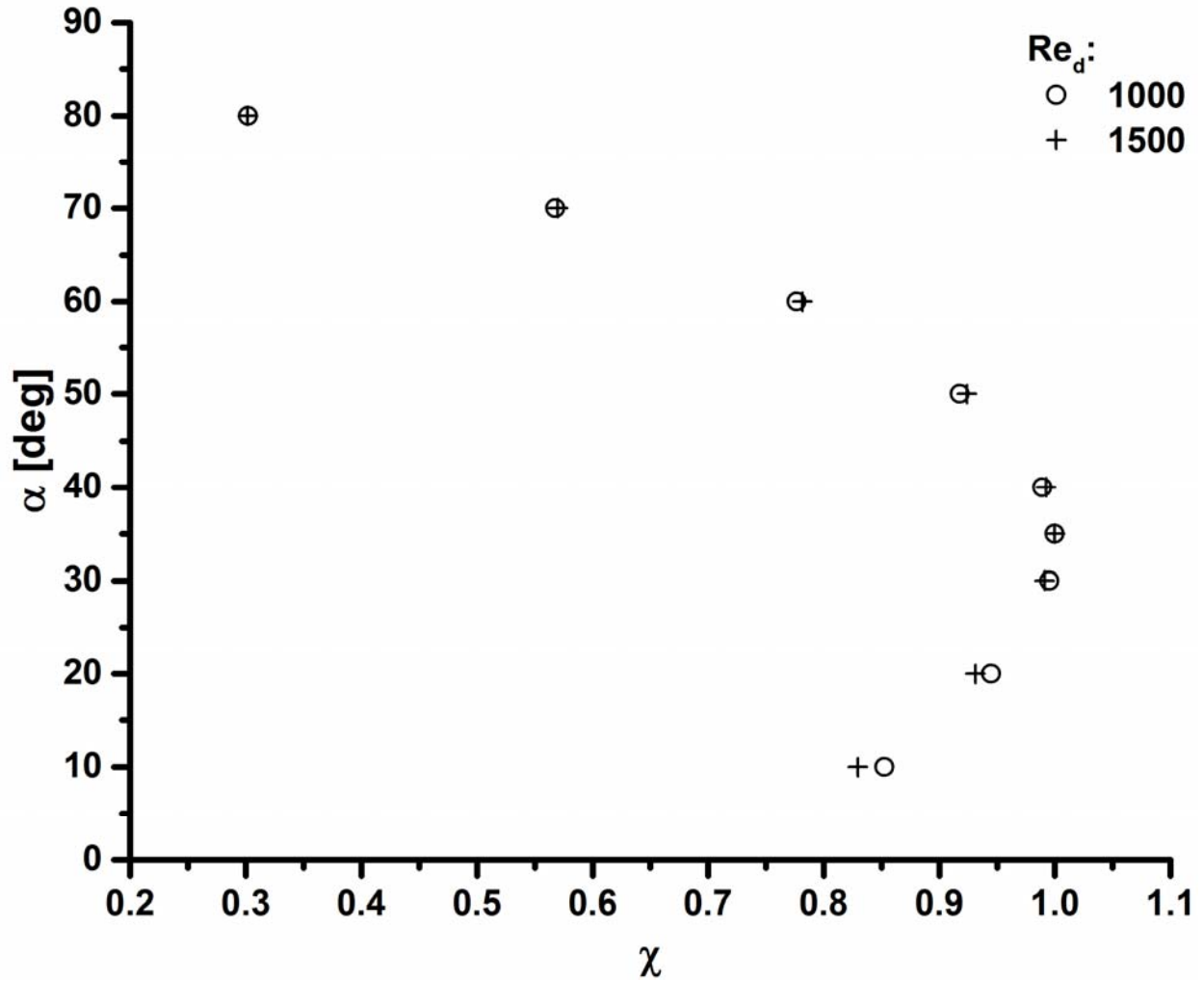


Fig. 6. Jet distance versus the initial inclination angle. The horizontal axis χ is the jet distance rendered dimensionless by the maximum value corresponding to $\alpha = 35^\circ$. The friction coefficient was $C_{fd} = 5Re_d^{-1/2 \pm 0.05}$.

5. Conclusion

Experiments conducted in this work with water jets combined with the predictions of the quasi-one-dimensional theory developed here revealed that the friction factor C_{fd} for the intact

curved free liquid jets moving in air is given by the following dependence on the Reynolds number, Re_d , based on the jet velocity, diameter and air viscosity: $C_{fd} = 5Re_d^{-1/2 \pm 0.05}$ (in the $621 \leq Re_d \leq 1289$ range). This dependence for the friction coefficient reveals the optimal inclination angle corresponding to the farthest reaching jet, $\alpha = 35^\circ$, which is in the agreement with previous experimental results. It should be emphasized that the established dependence $C_{fd} = C_{fd}(Re_d)$ is radically different from those established for melt spinning, where tiny filaments (of about 100 μm in diameter) move with velocities of the order of 1 km/min. Note that the present result $C_{fd} = 5Re_d^{-1/2 \pm 0.05}$ corresponds to jets of about 0.32 cm in diameter moving in air with velocities of about 4 m/s, and is applicable to jets originating from decorative fountains, smaller sprinklers, as well as to blood jets originating from knives or other cutting instruments used as a murder weapon, which is of interest in forensic applications.

6. References

- Arato EG, Crow DA, Miller DS (1970) Investigations of a high performance water nozzle. The British Hydromechanics Research Association. Tech. Rep. 1058.
- Ashgriz N, Yarin AL (2011) Capillary instability of free liquid jets. In: Ashgriz N (ed) Springer Handbook of Atomization and Sprays: Theory and Applications, Springer, Heidelberg, chapter 1, pp. 3-53.
- Basaran OA (1992) Nonlinear oscillations of viscous liquid drops. Journal of Fluid Mechanics 241: 169-198.

- Bilanski WK, Kidder EH (1958) Factors that affect the distribution of water from a medium-pressure rotary irrigation sprinkler. *Transaction of the ASAE* 1: 19-28.
- Clanet C (1998) On large-amplitude pulsating fountains. *Journal of Fluid Mechanics* 366: 333-350.
- Clanet C, Lasheras JC (1999) Transition from dripping to jetting. *Journal of Fluid Mechanics* 383: 307-326.
- Comiskey PM, Yarin AL, Kim S, Attinger D (2016) Prediction of blood back spatter from a gunshot in bloodstain pattern analysis. *Physical Review Fluids* 1: 043201.
- Comiskey PM, Yarin AL, Attinger D (2017a) Hydrodynamics of back spatter by blunt bullet gunshot with a link to bloodstain pattern analysis. *Physical Review Fluids* 2: 073906.
- Comiskey PM, Yarin AL, Attinger D (2017b) High-speed video analysis of forward and backward spattered blood droplets. *Forensic Science International* 276: 134-141.
- Comiskey PM, Yarin AL, Attinger D (2018) Theoretical and experimental investigation of forward spatter of blood from a gunshot. *Physical Review Fluids* (submitted).
- de Borda, J. C. *Mémoire sur l'écoulement des fluides par les orifices des vases*. *Mém. Acad. Sci. (Paris)*, 579–607 (1766).
- Federal Bureau of Investigation (2005) *Crime in the United States*. United States Department of Justice. <https://ucr.fbi.gov/crime-in-the-u.s/2014/crime-in-the-u.s.-2014>. Accessed 19 January 2018.
- Federal Bureau of Investigation (2014) *Crime in the United States*. United States Department of Justice. <https://www2.fbi.gov/ucr/05cius/>. Accessed 19 January 2018.

- Freeman JR (1889) Experiments relating to hydraulics of fire streams. Transactions of the American Society of Civil Engineers XXI: 303-461.
- Glicksman LR (1968) The cooling of optical fibres. Glass Technology 9: 131-138.
- Hanson D (2004) Bloodstain pattern analysis: Recreating the scene of the crime. Law Enforcement Technology 31: 84, 86-88, 90.
- Hatton AP, Osborne MJ (1979) The trajectories of large fire fighting jets. International Journal of Heat and Fluid Flow 6: 37-41.
- Hatton AP, Leech CM, Osborne MJ (1985) Computer simulation of the trajectories of large water jets. International Journal of Heat and Fluid Flow 6: 137-141.
- James SH, Kish PE, Sutton TP (2005) Principles of Bloodstain Pattern Analysis: Theory and Practice. CRC Press, Boca Raton.
- [Kochin](#) NE, [Kibel](#) IA, [Roze](#) NC. (1964) Theoretical Hydromechanics. John Wiley & Sons, New York.
- Kolbasov A, Comiskey PM, Sahu RP, Sinha-Ray S, Yarin AL, Sikarwar BS, Kim S, Jubery TZ, Attinger D (2016) Blood rheology in shear and uniaxial elongation. Rheologica Acta 55: 901-908.
- Lamb, H. (1959) Hydrodynamics. Cambridge University Press, Cambridge.
- Lin SP, Reitz RD (1998) Drop and spray formation from a liquid jet. Annual Review of Fluid Mechanics 30: 85-105.
- Lissaman PBS, Shollenberger CA (1970) Formation flight of birds. Science, 168: 1003-1005.
- Murzabaev MT, Yarin AL (1985) Dynamics of sprinkler jets. Fluid Dynamics 20: 715-722.

Rayleigh, Lord. 1878. On the instability of jets. Proc. Lond. Math. Soc. 10, 4-13.

Rouse HR, Howe JW, Metzler DE (1951) Experimental investigation of fire monitors and nozzles. Transaction of the American Society of Civil Engineers 77: 1147-1175.

Rutland DF, Jameson GJ (1971) A non-linear effect in the capillary instability of liquid jets. Journal of Fluid Mechanics 46: 267-271.

Schlichting, H. (1979) Boundary Layer Theory, McGraw-Hill, New York.

Tafreshi HV, Pourdeyhimi B (2003) The effects of nozzle geometry on waterjet breakup at high Reynolds numbers. Experiments in Fluids 35: 364-371.

Theobald C (1981) The effect of nozzle design on the stability and performance of turbulent water jets. Fire Safety Journal 4: 1-13.

Trettel B, Ezekoye OA (2015) Theoretical range and trajectory of a water jet. Proceedings of ASME 2015 International Mechanical Engineering Congress and Exposition. Rep. IMECE2015-52103.

Tuck EO (1976) The shape of free jets of water under gravity. Journal of Fluid Mechanics 76: 625-640.

Wahl TL, Frizell KH, Cohen EA (2008) Computing the trajectory of free jets. Journal of Hydraulic Engineering 134: 256-260.

Wonder AY (2001) Blood Dynamics. Academic Press, London.

Yarin AL (1992) Flow-induced on-line crystallization of rodlike molecules in fibre spinning. J. Applied Polymer Sci. 46: 873-878.

Yarin AL (1993) Free Liquid Jets and Films: Hydrodynamics and Rheology. Longman

Scientific & Technical and John Wiley & Sons, Harlow, New York, 1993.

Yarin AL (2011) Bending and buckling instabilities of free liquid jets: experiments and general quasi-one-dimensional model. In: Ashgriz N (ed) Springer Handbook of Atomization and Sprays: Theory and Applications, Springer, Heidelberg, chapter 2, pp. 55-73.

Yarin AL, Pourdeyhimi B, Ramakrishna S (2014) Fundamentals and Applications of Micro- and Nanofibers. Cambridge University Press, Cambridge.

Yarin AL, Roisman IV, Tropea C (2017) Collision Phenomena in Liquids and Solids. Cambridge University Press, Cambridge.

Ziabicki A (1976) Fundamentals of Fibre Formation. John Wiley& Sons, London.

Ziabicki A, Kawai H. (ed) (1985) High-Speed Fiber Spinning. John Wiley& Son, New York.